

# Role of Geometric Distortion and Polarization in Localizing Electronic Excitations in Conjugated Polymers

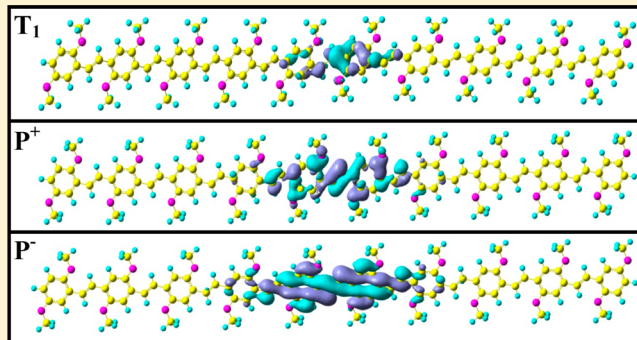
Iffat H. Nayyar,<sup>†,§,||</sup> Enrique R. Batista,<sup>†</sup> Sergei Tretiak,<sup>\*,†,‡</sup> Avadh Saxena,<sup>†</sup> Darryl L. Smith,<sup>†</sup> and Richard L. Martin<sup>†</sup>

<sup>†</sup>Theoretical Division and Center for Nonlinear Studies and <sup>‡</sup>Center for Integrated Nanotechnologies, Los Alamos National Laboratory, New Mexico 87545, United States

<sup>§</sup>NanoScience Technology Center and <sup>||</sup>Department of Physics, University of Central Florida, Orlando, Florida 32826, United States

## Supporting Information

**ABSTRACT:** Five different Density Functional Theory (DFT) models (ranging from pure GGA to long-range-corrected hybrid functionals) were used to study computationally the nature of the self-trapped electronic states in oligophenylene vinylenes. The electronic excitations in question include the lowest singlet ( $S_1$ ) and triplet ( $T_1^\dagger$ ) excitons (calculated using Time Dependent DFT (TD-DFT) method), positive ( $P^+$ ) and negative ( $P^-$ ) polarons, and the lowest triplet ( $T_1$ ) states (computed with the Self-Consistent Field (SCF) scheme). The polaron formation (spatial localization of excitations) is observed only with the use of range-corrected hybrid DFT models including long-range electronic exchange interactions. The extent of localization for all studied excitations is found to be invariant with respect to the size of the oligomer chain in their corresponding optimal geometries. We have analyzed the interdependence between the extent of the geometrical distortion and the localization of the orbital and spin density, and have observed that the localization of the  $P^+$  and  $P^-$  charged species is quite sensitive to solvent polarization effects and the character of the DFT functional used, rather than the structural deformations. In contrast, the localization of neutral states,  $S_1$  and  $T_1^\dagger$ , is found to follow the structural distortions. Notably,  $T_1$  excitation obtained with the mean field SCF approach is always strongly localized in range-corrected hybrid DFT models. The molecular orbital energetics of these excitations was further investigated to identify the relationship between state localization and the corresponding orbital structure. A characteristic stabilization (destabilization) of occupied (virtual) orbitals is observed in hybrid DFT models, compared to tight-binding model-like orbital filling in semilocal GGA functionals. The molecular and natural orbital representation allows visualization of the spatial extent of the underlying electronic states. In terms of stabilization energies, neutral excitons have higher binding energies compared to charged excitations. In contrast, the polaronic species exhibit the highest solvation energies among all electronic states studied.



## INTRODUCTION

Polymeric optoelectronic devices using semiconducting films of  $\pi$ -conjugated polymers are in much demand these days because of a variety of electronic and photonic applications in organic light emitting diodes,<sup>1,2</sup> solar cells,<sup>3–5</sup> lasers,<sup>6,7</sup> and field-effect transistors.<sup>8,9</sup> Investigations are being carried out to understand the operation of these devices, governed by the nature of the photoexcitations and the injection, transport, and recombination of charge carriers in the organic conjugated materials.<sup>10</sup> Three kinds of excitation processes play a vital role in the development of organic optoelectronic devices<sup>11</sup>: charge transfer by an electron or a hole, and excitonic energy transfer following the recombination of the electron and the hole, producing singlet and triplet excitations. The determination of the spatial extent of their structural and electronic wave function is vital for the detailed knowledge of the dynamics of the excitonic states.<sup>12–16</sup> It is, however, necessary to investigate

the ultrafast relaxation processes required in understanding the interplay between the efficient nonradiative transfer between excited states and the exciton dissociation into free electrons and holes (or polarons) giving rise to the photocurrent in semiconducting polymers.<sup>17,18</sup> Among all the polymers, the photophysical properties of PPV [poly (p-phenylene vinylene)] and its derivatives have been extensively studied because of their mechanical flexibility, simple and potential low-cost fabrication, superior luminescent properties,<sup>19,20</sup> and availability of extensive experimental measurements.<sup>21–23</sup>

Several experimental<sup>24–26</sup> and theoretical studies<sup>27–30</sup> performed earlier have highlighted the diffusion and mobility properties for excitons and polarons in substituted PPVs. Calculations have predicted the self-trapping of the electronic

Received: September 26, 2012

Published: December 3, 2012

excitations due to vibrational relaxation.<sup>31–34</sup> Also, neutral and charged excitation processes have been studied using time-dependent density functional theory (TD-DFT) for determining the electro-optical properties of PPV light emitting diodes.<sup>35</sup> The excitonic and polaronic sizes were found to be strongly dependent on the amount of orbital exchange included in the DFT functionals.<sup>36–38</sup> Norton et al.<sup>39</sup> studied the polarization effects on localized charge carriers using quantum mechanical/molecular mechanical (QM/MM) methods with a polarizable force field treating the environment as a dielectric continuum. However, Dykstra et al.<sup>12</sup> demonstrated, via semiempirical methods, the localization of the excitons as due to the dynamic relaxation in 2-methoxy-5-(2'-ethyl-hexyloxy)-*p*-phenylenevinylene (MEH-PPV). In our previous communication,<sup>40</sup> we benchmarked the ability of the current functional approximations to describe the extent of the self-trapped neutral and charged electronic excitations for MEH-PPV. We reported the significant role played by the amount of long-range orbital exchange in the density functional and the surrounding dielectric environment in studying the spatial confinement of these wave functions in agreement with several experimental and theoretical studies.<sup>22,31,33,41–43</sup> In particular, only DFT models carrying a significant portion of orbital exchange are able to reproduce the recent experimental observation<sup>41</sup> that the polaronic spin density in MEH-PPV is spread roughly only over 10 C–H bonds (2–3 repeat units), which is consistent with an earlier experimental estimate ( $\sim$ 4 phenyl rings)<sup>43</sup> obtained via electron–nuclear double resonance (ENDOR) studies. The range-corrected functional LC-wPBE with full orbital exchange at long-range predicted localized polaron formation in both the presence and the absence of the polarizable medium whereas the half-and-half functional BHandHLYP produces significant localization in charged polymers only in the presence of a dielectric environment. A time-dependent study for the excited electronic states has laid emphasis on the role played by the Coulomb interactions in the localization of the polarons and excitons.<sup>44</sup> Recently Sai et al.<sup>45</sup> predicted polaron formation in perfect molecular crystals by tuning the fraction of exact exchange in hybrid DFT by first principles. A previous study<sup>46</sup> of the impact of various theoretical methods on the geometric and electronic properties of unsubstituted oligo (phenylene vinylene) (OPV) radical cations has exposed a sensitivity on the choice of the method rather than on the molecular structure. Zojer et al.<sup>47</sup> have investigated the geometry relaxation effects following the electronic excitations to locate the regions of the strongest rearrangement of the electron density in conjugated organic molecules. Further, polaron formation has been observed in the presence of a polarizing environment in a nonadiabatic study of exciton dissociation in PPV oligomers.<sup>48</sup> Frolov et al.<sup>49</sup> spectroscopically investigated properties of the  $\pi$ – $\pi^*$  transitions in PPV derivatives in the photoinduced absorption bands.

All these studies performed in the past indicate two distinct origins leading to self-localization (or self-trapping) of electronic excitations in low-dimensional semiconducting polymers. First of all, distortion of molecular geometry may create a spatially localized potential energy well where the state wave function self-traps. Second, even in the absence of geometric relaxation and vibrational dynamics, the electronic excitation may become spatially confined due to energy stabilization caused by polarization effects from the surrounding dielectric medium. This motivated us to conduct a detailed first

principle study of oligo (phenylene vinylene) derivatives aiming to separate these two fundamental sources of spatial localization. This is important for understanding excited-state dynamics and charge-transfer properties of excitons and polarons in polymeric materials.

In this paper, we present a study of five different excited states of the PPV oligomer, calculated with a broad spectrum of computational tools. Building on our previous communication,<sup>40</sup> which has emphasized the importance of long-range corrections for the proper description of these excitations, here we examine in detail the interplay of geometrical distortion and polarization on the delocalization of these electronic states in reference to the excited state localization, binding energy, molecular orbital structure, and solvation energy.

## ■ COMPUTATIONAL METHODOLOGY

We study the ground state  $S_0$  (charge = 0, spin = 0), positive polaron  $P^+$  (charge = +1, spin = 1/2), negative polaron  $P^-$  (charge = -1, spin = 1/2), first triplet  $T_1$  (charge = 0, spin = 1), first singlet  $S_1$  (charge = 0, spin = 0), and first triplet  $T_1^\dagger$  (charge = 0, spin = 1) excited states for a ten-repeat-unit MEH-PPV oligomer in its trans-isomeric geometrical form unless otherwise mentioned. In our model, the side-chain groups  $OC_8H_{17}$  in MEH-PPV have been replaced by  $OCH_3$  to speed up the quantum calculations. Every repeat unit consists of a phenyl ring attached to a vinyl linkage. The two terminal rings share the same vinyl bridge. Cationic  $P^+$  and anionic  $P^-$  species correspond to the presence of a hole and an electron on the chain, respectively. Optimal geometries and energetics of  $P^+$ ,  $P^-$ , and  $T_1$  states are obtained using the standard self-consistent force (SCF) scheme, whereas  $T_1^\dagger$  and  $S_1$  are calculated using TD-DFT methodology. In particular, this allows us to compare properties of the first triplet state obtained with two different computational techniques: the variational mean-field SCF approach for a given spin state (denoted as  $T_1$ ) and the TD-DFT method for calculating the triplet state (denoted as  $T_1^\dagger$ ) via single-particle excitations from the reference ground state  $S_0$ .

A moderately polar solvent, acetonitrile ( $\epsilon = 35.7$ ), is included in this study via the conductor-like polarizable continuum model (CPCM) as implemented in the Gaussian09 software package<sup>50</sup> to mimic the polymer's highly polarizable dielectric environment. Even though this may be an overestimation of the dielectric constant of PPV,<sup>51</sup> the effects of this dielectric medium throughout our study are minor, and the conclusions are the same as for the simulations in gas phase. All computations have been performed using the Gaussian09 suite<sup>50</sup> and the 6-31G\* basis set. Fully relaxed geometries of all the six electronic states ( $S_0$ ,  $P^+$ ,  $P^-$ ,  $T_1$ ,  $S_1$ , and  $T_1^\dagger$ ) are studied at five different DFT levels without imposing any symmetry constraints. These DFT levels are composed of different exchange-correlation (XC) functionals, namely, PBE<sup>52</sup> ( $a = 0$ ), B3LYP<sup>53</sup> ( $a = 20$ ), BHandHLYP<sup>53</sup> ( $a = 50$ ), CAM-B3LYP<sup>54</sup> ( $a = 20$ –65), and LC-wPBE<sup>55</sup> ( $a = 0$ –100), where parameter  $a$  is the fraction of Hartree–Fock (HF) exchange in the XC functional given as

$$E_{XC} = aE_X^{\text{HF}} + (1 - a)E_X^{\text{GGA}} + E_C^{\text{GGA}} \quad (1)$$

The long-range-corrected functionals behave as the typical hybrid or generalized gradient approximation (GGA) at short-range. However, they have an increasing HF component at

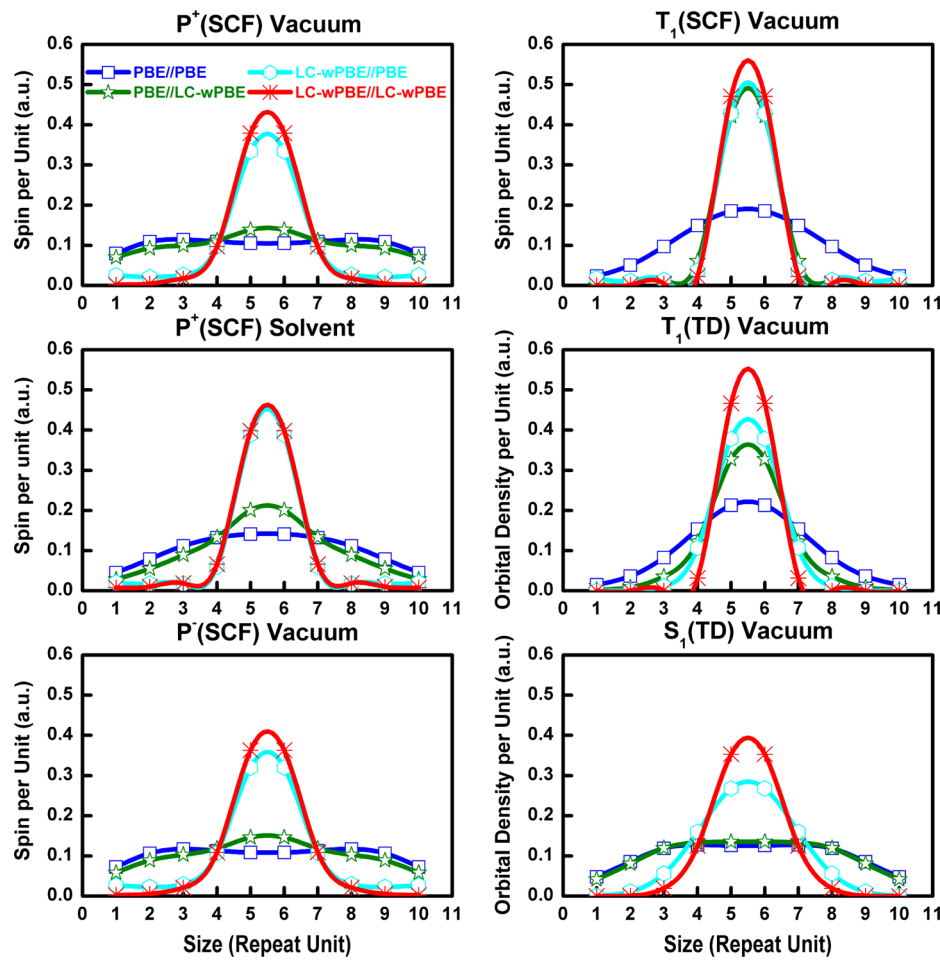


**Figure 1.** Electronic density per repeat unit (a.u.) of the MEH-PPV oligomer consisting of 10 repeat units computed at PBE//PBE, PBE//LC-wPBE, LC-wPBE//PBE, and LC-wPBE//LC-wPBE levels using a 6-31G\* basis set for five electronic states: positive ( $P^+$ ) and negative ( $P^-$ ) polarons, the first triplet ( $T_1$ ) excited state obtained using the SCF scheme, and the first triplet ( $T_1^\dagger$ ) and singlet ( $S_1$ ) excitons calculated using TD-DFT methodology. Plotted are the Mulliken atomic spin densities (spin per unit) integrated over each repeat unit for  $P^+$ ,  $P^-$ , and  $T_1$  states, and the average population densities of the NTOs for the hole and electron (orbital density per unit) for  $T_1^\dagger$  and  $S_1$  excitations. The spin and orbital densities are normalized to unit for fair comparison and are calculated using the first functional in the legend in their corresponding fully relaxed geometries optimized with the second functional.

longer distances up to a maximum value, 65% for CAM-B3LYP and 100% for LC-wPBE.

Comparison of bond length alternations<sup>56</sup> (BLAs) and electronic density distributions<sup>37,57</sup> in conjugated organic polymers is useful in understanding the factors governing localization in them. On one hand, BLA predicts the degree of structural deformation and, thus, confinement of the state wave function arising due to the distortion during geometry relaxation. However, the electron density distribution directly signifies spatial confinement of this wave function on the distorted or undistorted geometry. To quantify two distinct origins of excitation localization and to explore the interrelation between them, we calculate the electronic density at PBE and LC-wPBE levels for both uniform and distorted geometries separately. In our previous publication,<sup>40</sup> we observed that the long-range-corrected LC-wPBE exhibited clear structural and electronic localization in contrast to the pure GGA functional PBE. Long-range-corrected hybrid functionals have been shown to predict the BLAs and charge-transfer excitations in  $\pi$ -conjugated materials.<sup>58,59</sup> To investigate the effect of geometry distortion on the electronic localization we show the electronic calculations at PBE level for both PBE and LC-wPBE optimized

geometries. Similarly, the LC-wPBE level of calculation for both these geometries allows us to infer the influence of the delocalized geometry on the localization of the electronic wave function. The Mulliken atomic spin densities (difference in the spin of electrons in alpha and beta molecular orbitals, MOs) integrated over each repeat unit for all the SCF excitations are used to measure the delocalization of the electronic state for polaronic states, and the same analysis on the natural transition orbitals<sup>60</sup> (NTOs) of a hole or electron yields information about the localization of excited states in neutral TD-DFT excitations. Since the hole and electron orbital wave functions show similar delocalization properties (in the absence of charge-transfer states in these polymeric chains) the average of the two is analyzed. The spin and orbital densities for all these excitations are normalized to unity for a fair comparison.

## RESULTS AND DISCUSSION

Figure 1 summarizes the effect of the DFT model on the localization properties of electronic excitations by showing the distribution of the Mulliken atomic spin density (electronic density per repeat unit) along the chain for a ten-repeat-unit MEH-PPV oligomer. In Figure 1 we have used a composite

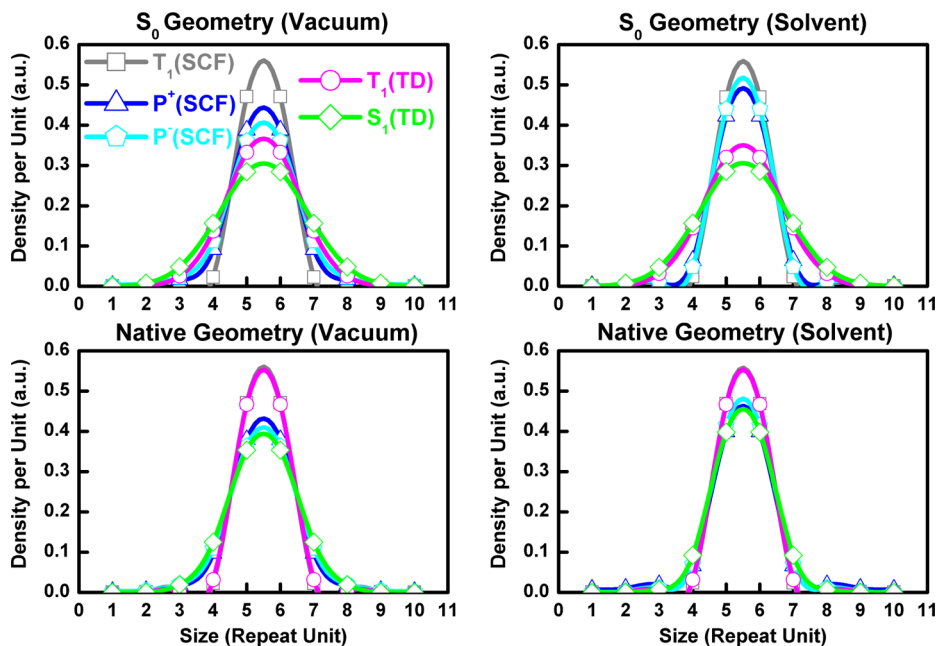


**Figure 2.** Electronic density per repeat unit (a.u.) of the MEH-PPV oligomer consisting of 10 repeat units for all the excitations ( $T_1$ ,  $P^+$ ,  $P^-$ ,  $T_1^\dagger$ , and  $S_1$ ) in ground state ( $S_0$ ) geometry (top panel) and their corresponding native geometries (bottom panel) calculated at the LC-wPBE level using a 6-31G\* basis. Both vacuum (left) and solvent (right) calculations are shown. Plotted electronic density has been calculated as specified in the caption to Figure 1.

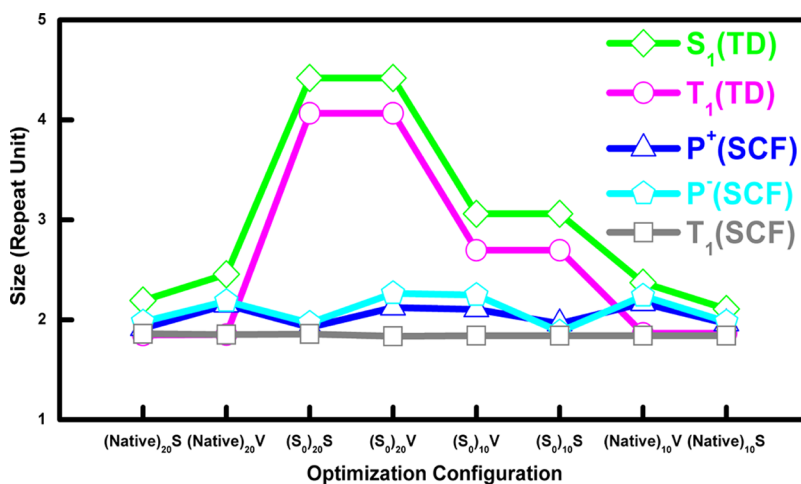


**Figure 3.** Characteristic size of calculated electronic excitations ( $S_1$ ,  $T_1^\dagger$ ,  $P^+$ ,  $P^-$ , and  $T_1$ ) defined as the full width at half-maximum (fwhm) in terms of the repeat units in MEH-PPV oligomers of different lengths calculated at the LC-wPBE level. The  $x$ -axis label of this figure describes the geometry in a common bracket with the number of repeat units of the polymer as a subscript, and the medium (V and S stand for vacuum and solvent, respectively).

notation “functional1//functional2” that indicates, first the DFT models used for the calculation of the spin (or orbital) density, and second the functional used to obtain the geometry of the molecule. Previously we found<sup>40</sup> that semilocal PBE and range-corrected LC-wPBE functionals result in “uniform” and “distorted” optimal geometries, respectively, corresponding to delocalized and localized excitation. Here we observe that the  $P^+$  polaron spin density calculated using the PBE (LC-wPBE) model in vacuum remains delocalized (localized) irrespective of what geometry one uses (see Figure 1). Consequently, the localization of the  $P^+$  charged state is driven by the character of the functional rather than by structural distortions. Compared to an isolated molecule, the localization of the  $P^+$  excitation increases when polarizable dielectric medium effects are

included in the calculations. The  $P^-$  excitation behaves very much as  $P^+$ . Thus, particle-hole symmetry is conserved in a uniform all-trans MEH-PPV oligomer, and the LC-wPBE model always localizes this excitation. However, the geometry distortion at the LC-wPBE optimal geometry is local and strong (the respective BLA becomes negative<sup>40</sup>), so that the  $T_1$  state becomes localized even at the PBE level when the LC-wPBE optimal geometry is used (Figure 1). Triplet state localization calculated with the TD-DFT approach shows the same trend as the calculation at the mean-field SCF level. Notably, localization properties of the first excited state  $S_1$  calculated using TD-DFT seem to be similar to those of the  $P^+$  state (except a slightly larger size). However, this conclusion is not justified since in this case the end effects appear and calculations of

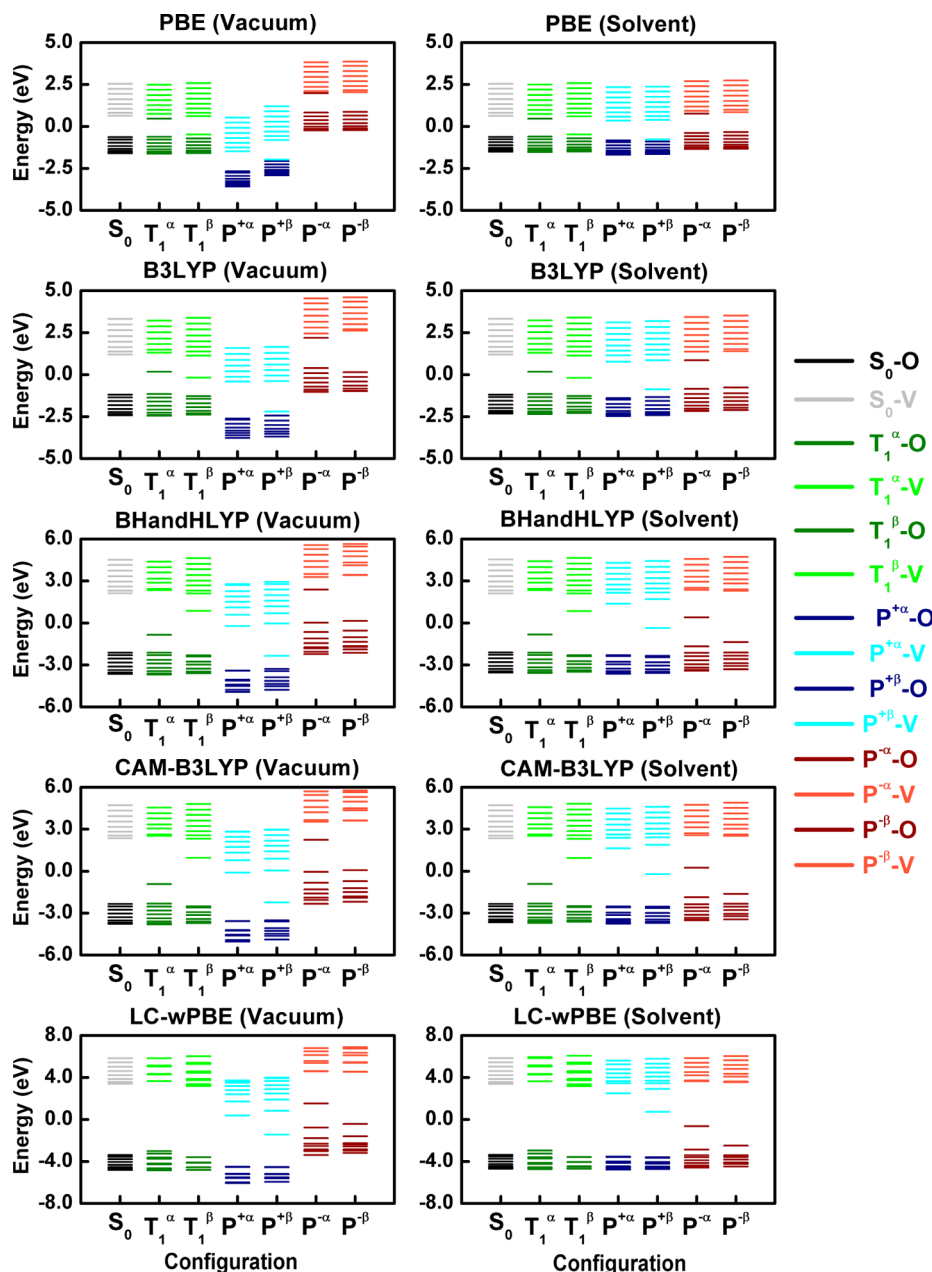


**Figure 4.** Density of Kohn–Sham states of a MEH-PPV oligomer composed of 10 repeat units computed using various functional models with a 6-31G\* basis set for the  $S_0$ ,  $T_1$ ,  $P^+$ , and  $P^-$  states calculated using SCF. The alpha ( $\alpha$ ) and beta ( $\beta$ ) molecular orbitals (MOs) of each spin state are shown separately (represented by the same color). The darker (lighter) shades in the figure correspond to the occupied (O) and virtual (V) orbitals, respectively. Both vacuum (left) and solvent (right) calculations are shown.

larger oligomers are necessary (see the discussion below). The calculations for neutral  $T_1$ ,  $T_1^\dagger$ , and  $S_1$  excitations in a dielectric medium are not shown in Figure 1 as they offer no substantial effect on their localization properties.

Figure 2 explores the effect of the geometry relaxation on the localization of the state wave function calculated for the ten-repeat-unit MEH-PPV oligomer. Plotted are spin (for SCF calculations) and orbital (for TD-DFT calculations) electronic densities for all excitations ( $T_1$ ,  $P^+$ ,  $P^-$ ,  $T_1^\dagger$ , and  $S_1$ ) in the ground state  $S_0$  “uniform” geometry (top row) and in their corresponding native optimal “distorted” geometries (bottom panel) as calculated at LC-wPBE level. In vacuum, we observe that  $T_1$  is much more localized than  $P^+$  and  $P^-$ —a more quantitative measure of localization/delocalization is given in

Figure 3. The  $P^+$  localization is similar to that of  $P^-$ . The  $T_1$  state computed with the SCF is much more localized compared to  $T_1^\dagger$ . This difference in results between SCF and TD-DFT calculations is discussed below. The  $S_1$  state exhibits the least tendency to localize among them all. Further addition of a polarizable medium (solvent) into the calculation localizes the charged ( $P^+$  and  $P^-$ ) species but has no effect on the neutral ( $T_1$ ,  $T_1^\dagger$ ,  $S_1$ ) states. The bottom panels in Figure 2 display the electronic localization of the excitations under study in their corresponding relaxed native geometries. Comparing top and bottom panels we see that the geometry relaxation has no influence on the  $T_1$ ,  $P^+$ , and  $P^-$  excitations since they are already strongly localized at the undistorted  $S_0$  geometry. However, the  $T_1^\dagger$  and  $S_1$  states calculated with TD-DFT are

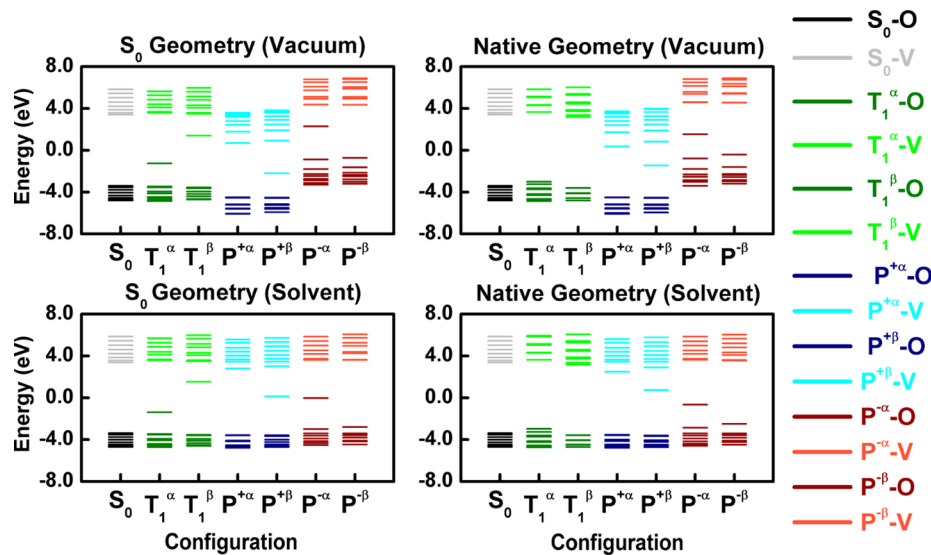


**Figure 5.** Density of Kohn–Sham orbitals for  $S_0$ ,  $T_1$ ,  $P^+$ , and  $P^-$  states of the MEH-PPV oligomer composed of 10 repeat units computed at the LC-wPBE/6-31G\* level for the  $S_0$  state geometry (left panel) and their corresponding native optimal geometries (right panel). The alpha ( $\alpha$ ) and beta ( $\beta$ ) molecular orbitals (MOs) of spin states are shown separately (represented by the same color). The darker (lighter) shades in the figure correspond to the occupied (O) and virtual (V) orbitals, respectively. Both vacuum (top panel) and solvent (bottom panel) calculations are shown.

found to be much more localized in their corresponding native geometries than in the  $S_0$  state: the  $S_1$  state being nearly as localized as  $P^+$  and  $P^-$ , whereas  $T_1^\dagger$  localization coincides with that of  $T_1$ . This indicates a significant localization effect associated with geometry distortion for the neutral  $T_1^\dagger$  and  $S_1$  excitations within the TD-DFT framework. Given strong localization of all states, the solvent effects are minimal in their corresponding relaxed geometries (Figure 2). A figure similar to Figure 2 calculated at the BHandHLYP level is shown in the Supporting Information, Figure 1S emphasizing the generality of our observations.

The localization properties predicted by the LC-wPBE functional in terms of the characteristic size of the electronic excitations for  $S_0$  and corresponding native geometries in vacuum and solvent are summarized in Figure 3 for 10 and 20 repeat units of the MEH-PPV oligomer. This size is defined as the full width at half-maximum (fwhm) in terms of the repeat units of the electronic density plots of the polymer chain. The triplet state  $T_1$  exhibits the highest localization for all states considered in Figure 3 being insensitive to the chain length, solvent, and geometric distortion. Polarization of the medium plays an important role in the localization of the charged ( $P^+$  and  $P^-$ ) species, while distortions of geometry have smaller effects. It is clearly evident from Figure 3 that the singlet state  $S_1$  is more delocalized than the triplet state  $T_1$  for all cases as one would expect because of the Pauli repulsion of the two electrons occupying the same orbital. It is also observed in the Karabunarliew et al.<sup>33</sup> study and argued to be due to the absence of repulsive spin-exchange between the electron and the hole. As expected, the localization sizes do not depend on the oligomer length for all calculations of  $T_1$ ,  $P^+$ , and  $P^-$  excitations performed at the mean-field SCF level. However, the situation is different for TD-DFT calculations of  $T_1^\dagger$  and  $S_1$  states. We observe a strong increase of  $T_1^\dagger$  size at the uniform ground state  $S_0$  geometry when doubling the size of the oligomer from 10 to 20 repeat units, which is drastically different from the SCF results for the  $T_1$  state. This difference can be attributed to the fact that, for a uniform geometry, TD-DFT builds the excited state wave function by an equal weight superposition of

the single-particle excitations from the ground state along the chain (i.e., the delocalization of  $T_1^\dagger$  state would monotonically grow with the chain length).<sup>46,61</sup> In contrast, the mean-field construct automatically limits the spatial extent of a spin to fewer than two repeat units. However, it is important that geometry distortion is local and one has a strongly localized triplet state at the TD-DFT level. Namely, triplets  $T_1$  and  $T_1^\dagger$  do show the same extent of localization in their corresponding native geometries, demonstrating consistency between SCF and TD-DFT modeling. Calculations of the first singlet excitation  $S_1$  with the TD-DFT approach show trends similar to  $T_1^\dagger$  modeling. Notably, the dielectric medium slightly increases  $S_1$  localization for native geometry (exciton self-trapping).

We further examine the density of single-particle states (Kohn–Sham orbitals) for all SCF calculations ( $S_0$ ,  $T_1$ ,  $P^+$ , and  $P^-$ ) in their corresponding native geometries calculated at the PBE, B3LYP, BHandHLYP, CAM-B3LYP, and LC-wPBE levels in Figure 4. Calculation of ground state  $S_0$  shows a typical highest occupied molecular orbital (HOMO) to lowest unoccupied molecular orbital (LUMO) gap between occupied and valence space growing with an increase of the orbital exchange in the functional model. In the semilocal PBE framework, all excitations ( $T_1$ ,  $P^+$ , and  $P^-$ ) are formed by filling/emptying the respective orbitals with minimal change in the relative orbital energetics. For example, the  $T_1$  state is obtained by promoting an electron from the  $\beta$  HOMO to the  $\alpha$  LUMO. Thus, pure/semilocal DFT behaves as a typical tight-binding model with no electronic orbital relaxation effects. Calculation of charged species  $P^+$  ( $P^-$ ) in vacuum leads to stabilization (destabilization) of the entire orbital manifold as evidenced by shifts down (up) in Figure 4 (left column). Notably, calculations of  $P^+$  and  $P^-$  in the solvent environment strictly align their HOMO–LUMO gaps with the respective neutral species  $S_0$  and  $T_1$  (Figure 4, right column). In addition, the solvent leads to a slight increase in the band gap for the charged ( $P^+$  and  $P^-$ ) excitations as compared to their respective counterparts in the vacuum. This is consistent with earlier DFT results on the effect of polarization functions on large systems with  $\pi$ -conjugation.<sup>62,63</sup> Adding a fractional amount of

**Table 1.** Binding Energies of the 10 Repeat Unit MEH-PPV Oligomer for All the SCF ( $T_1$ ,  $P^+$  and  $P^-$ ) and TD-DFT ( $S_1$  and  $T_1^\dagger$ ) Excitations under Study at Five Different XC Functionals<sup>a</sup>, Both in Vacuum (V) and Solvent (S)

	Binding Energy [ $E(S_0X) - E(X,X)$ ] (eV)									
	excitation (X)									
	$T_1$		$P^+$		$P^-$		$S_1$		$T_1^\dagger$	
	V	S	V	S	V	S	V	S	V	S
PBE	0.10	0.10	0.03	0.03	0.04	0.04	0.06	0.06	0.10	0.10
B3LYP	0.30	0.29	0.05	0.06	0.06	0.07	0.13	0.14	0.20	0.20
BHandHLYP	0.67	0.66	0.11	0.18	0.11	0.19	0.18	0.19	1.39	1.38
CAM-B3LYP	0.63	0.62	0.14	0.17	0.14	0.19	0.17	0.17	1.31	1.29
LC-wPBE	1.01	0.99	0.29	0.26	0.31	0.28	0.30	0.30	1.81	1.80

<sup>a</sup>XC functionals: PBE, B3LYP, BHandHLYP, CAM-B3LYP, and LC-wPBE. The difference between the total energy of the excitation (X) in  $S_0$  geometry and that in its corresponding fully relaxed geometry is reported. Binding energies in italics are not meaningful because of the negative excitation energies from the  $S_0$  state attributed to the orbital instabilities introduced with higher HF exchange.

Hartree–Fock (HF) orbital exchange into the DFT functional results in a well-pronounced electronic orbital relaxation, that is, the singly occupied state shifts down toward the occupied manifold whereas the singly unoccupied state moves up toward the valence manifold. The solvent enhances this stabilization. Consequently, for a range-corrected LC-wPBE model (with 100% of asymptotic exchange) calculations of  $T_1$  in solvent, ( $n + 1$ )  $\alpha$  and ( $n - 1$ )  $\beta$  occupied orbitals become well aligned and well separated from the respective virtual orbitals. Calculations at the same level of the charged state  $P^+$  ( $P^-$ ) lead to the appearance of a single unoccupied (occupied) state located close to the midgap. This is a typical picture of polaron energetics emerging from solid-state models.<sup>30,64,65</sup> Optical transitions emerging after creating charge carriers are attributed to such states and have been extensively explored via ultrafast pump–probe spectroscopy.<sup>23,49,66</sup>

Figure 5 elucidates the effects of geometry relaxation on the energy band picture for these ( $S_0$ ,  $T_1$ ,  $P^+$ , and  $P^-$ ) states calculated at the LC-wPBE level. As shown in our previous publication<sup>40</sup> compared to the  $S_0$  uniform geometry, the BLA parameter calculated with the LC-wPBE functional is locally reduced in the middle of the molecule at the respective native optimal geometry indicating excitation self-trapping. This distortion increases from the  $S_1$  state to charged  $P^+$  and  $P^-$  species, and to even inverted (negative) BLA for the  $T_1$  excitation. Such strong geometry distortion for the  $T_1$  state manifests itself by a visible orbital relaxation of the midgap singly occupied  $\alpha$  and empty  $\beta$  levels in the  $S_0$  geometry toward the respective occupied and virtual manifolds at the native geometry. In contrast, positions of Kohn–Sham orbitals are not significantly affected by geometry relaxation for charged states  $P^+$  and  $P^-$ . Compared to vacuum, the solvent environment aligns the band-gaps of charged excitations with the neutral ones and further facilitates the orbital relaxation. Supporting Information, Figure 2S displays similar plots obtained for the other 3 functionals, PBE, B3LYP, and CAM-B3LYP (only vacuum calculations are shown), illustrating a monotonic reduction of the orbital relaxation with decrease of the orbital exchange fraction in the DFT kernel.

This analysis of the orbital energetics allows us to rationalize trends in the excitation binding energies due to geometry relaxation (Table 1) and solvation energies (Table 2). Table 1 summarizes the binding energies calculated for the 10 repeat unit MEH-PPV oligomer for all excitations ( $T_1$ ,  $P^+$ ,  $P^-$ ,  $S_1$ , and  $T_1^\dagger$ ) under study at various DFT levels both in vacuum and in solvent. Binding energy is defined as the difference between the

**Table 2.** Solvation Energies of the 10 Repeat Units of the MEH-PPV Oligomer for All the SCF ( $T_1$ ,  $P^+$  and  $P^-$ ) and TD-DFT ( $S_1$  and  $T_1^\dagger$ ) Excitations under Study at Five Different XC Functionals<sup>a</sup>

	Solvation Energy [ $E(S_0X_V) - E(S_0X_S)$ ] (eV)				
	excitation (X)				
	$T_1$	$P^+$	$P^-$	$S_1$	$T_1^\dagger$
PBE	1.65	1.85	2.68	1.68	1.65
B3LYP	1.57	1.82	2.64	1.61	1.56
BHandHLYP	1.66	2.10	2.95	1.71	1.63
CAM-B3LYP	1.59	2.11	2.93	1.64	1.58
LC-wPBE	1.78	2.46	3.35	1.83	1.75

<sup>a</sup>XC functionals: PBE, B3LYP, BHandHLYP, CAM-B3LYP, and LC-wPBE. The difference between the total energy of the excitation (X) in vacuum and that in the solvent is reported. Both these energies are calculated in the  $S_0$  geometry.

total energy of the excitation in the neutral ( $S_0$ ) geometry and that in its fully relaxed configuration (denoted as X). Binding energy is an important parameter controlling the charge transport in conjugated polymers.<sup>67</sup> Overall, we observe a gradual increase in the energy with the percent of HF exchange in the functionals for all excitations (Table 1). The semilocal PBE model with zero HF exchange produces the lowest, heavily underestimated energies among all,<sup>68,69</sup> whereas the LC-wPBE functional with full HF exchange at the long-range reports the highest energies. The values calculated at BHandHLYP with 50% HF exchange and coulomb attenuated CAM-B3LYP are almost the same. Addition of a dielectric medium does not have a significant effect on these energies. At the LC-wPBE level, the binding energy of the triplet state  $T_1$  is the largest, reflecting significant electronic orbital relaxation (Figure 4) due to large geometry distortion. Binding energies for the  $P^+$ ,  $P^-$ , and  $S_1$  excitations are about the same. Notably, binding energies for the  $T_1^\dagger$  excitation calculated using TD-DFT with functionals with high fraction of orbital exchange (BHandHLYP, CAM-B3LYP, and LC-wPBE) are not meaningful because of the negative excitation energies from the  $S_0$  state (marked in the italic red). This is a manifestation of the well-known triplet instability first observed in the time-dependent Hartree–Fock methodology, which also appears in TD-DFT for hybrid functionals with large amount of HF exchange, as studied in detail elsewhere.<sup>58</sup> These problems arise when a spin-contaminated unrestricted Kohn–Sham solution becomes

lower in energy than the respective restricted closed-shell solution.<sup>58</sup>

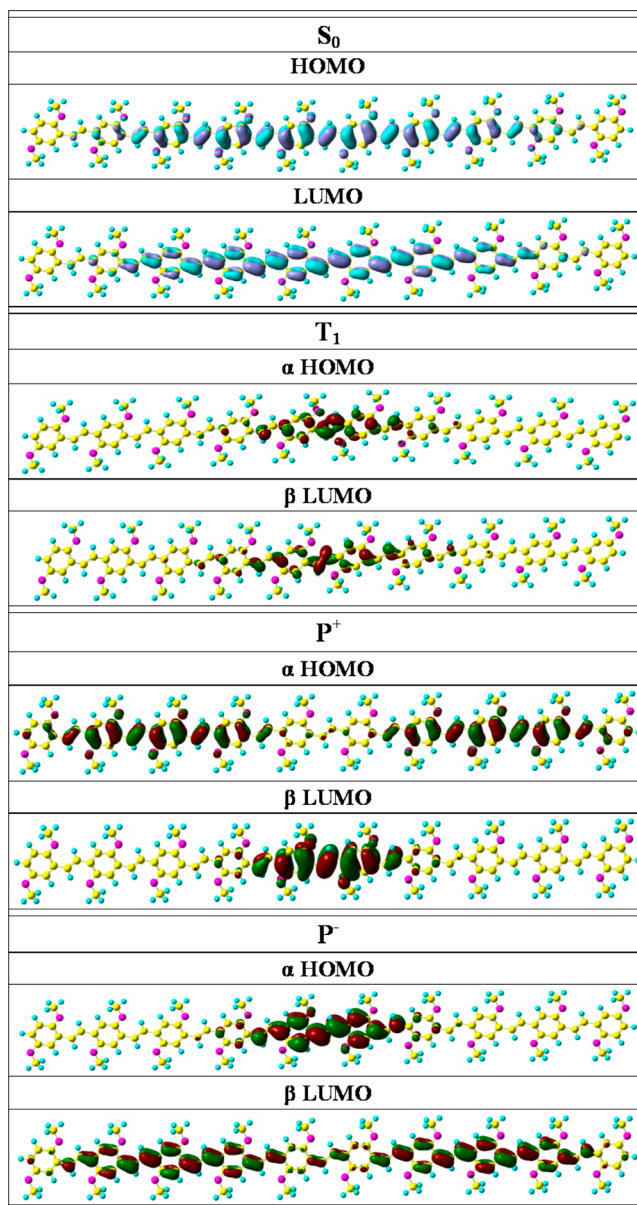
Table 2 reports the solvation energies for the 10 repeat unit MEH-PPV oligomer for all excitations ( $T_1$ ,  $P^+$ ,  $P^-$ ,  $S_1$ , and  $T_1^\dagger$ ) under study calculated at various DFT levels. This quantity is defined as the difference between the total energy of the excitation in vacuum and that in the solvent, both calculated using the  $S_0$  geometry. Overall solvation energies are significant, varying from 1.5 to 3 eV across the set. Their values gradually increase with an increase of the fraction of orbital exchange in the functional owing to a larger solvent stabilization of more localized states. The solvation energies for the polaronic species  $P^+$  and  $P^-$  are markedly higher than those for neutral ones ( $T_1$ ,  $S_1$ , and  $T_1^\dagger$ ) because of the orbital alignment effect shown in Figure 4.

Figure 6 displays the characteristic HOMO and LUMO orbitals for  $S_0$ ,  $T_1$ ,  $P^+$ , and  $P^-$  states in their corresponding native geometries calculated using the LC-wPBE model in the presence of the solvent. For all the states but  $S_0$ , the highest energy valence state belongs to  $\alpha$  orbitals whereas the lowest energy conduction state to the  $\beta$  orbitals. We observe the HOMO and the LUMO for  $S_0$  to be delocalized throughout the oligomer whereas those for the  $T_1$  state become completely localized because of a significant geometry distortion. The  $\alpha$  HOMO of  $P^-$  represents a localized state of a negative polaron, whereas the  $\beta$  LUMO orbital is delocalized. The situation is reversed for  $P^+$  excitation, where the  $\beta$  LUMO represents a polaronic state. A similar plot, but for calculations in vacuum presented in the Supporting Information, Figure 3S, shows that the solvent does not change the form/delocalization of the orbitals.

Finally, orbital analysis of electronic excitations can be conducted using the natural orbital (NO) representation for the singly occupied electronic levels as shown in Figure 7 for  $T_1$ ,  $P^+$ , and  $P^-$  excitations calculated at the LC-wPBE level in the presence of the polarizable dielectric medium. These NOs are defined as the eigenfunctions of the spinless one-particle electron density matrix. The  $T_1$  state has only two orbitals with a single occupation as shown in the figure whereas  $P^+$  and  $P^-$  have only one NO with unit occupation. These plots visually show that the localization of the  $T_1$  state is more pronounced compared to  $P^+$  or  $P^-$  excitations. Similar plots obtained for calculations in vacuum are shown in the Supporting Information, Figure 4S.

## CONCLUSIONS

In summary, we presented a detailed computational study and analysis of the energetics and spatial delocalization of significant electronic states in conjugated oligomers (phenylene vinylenes), thus providing a deeper understanding of the physics controlling localized excitations in organic electronic materials for technological applications. Use of the long-range-corrected DFT functionals, such as LC-wPBE, is found to be crucial to predict physically correct spatial localization of all electronic excitations considered. In these models, we observe that the electronic localization of charged  $P^+$  and  $P^-$  states is mostly decided by polarization properties of the surrounding media, while exhibiting lesser dependence on the molecular geometry. However, localization of the neutral  $S_1$  and  $T_1$  ( $T_1^\dagger$ ) states is weakly dependent on polarization. For these excitations, the self-trapping of their electronic wave functions mostly follows the lattice distortion when the TD-DFT methodology is used. In particular, TD-DFT calculated  $S_1$  and  $T_1^\dagger$  excitations are



**Figure 6.** Characteristic HOMO and LUMO molecular orbitals of  $S_0$ ,  $T_1$ ,  $P^+$ , and  $P^-$  states in their corresponding native geometries calculated at the LC-wPBE/6-31G\* level in the presence of solvent for the MEH-PPV oligomer composed of 10 repeat units. For all states but  $S_0$ , the HOMO and LUMO represent alpha ( $\alpha$ ) and beta ( $\beta$ ) electrons, respectively.

found to be strongly delocalized along the oligomer chain at the uniform ground state  $S_0$  geometry, owing to the nonvariational construction of the excited state wave function. In contrast, mean-field calculated  $P^+$ ,  $P^-$ , and  $T_1$  states are always spatially localized even in the  $S_0$  geometry, independent of the oligomer length used. Polaron  $P^+$  and  $P^-$  formation is signified by the presence of localized states for the hole or the electron deep inside the HOMO–LUMO gap of the oligomer because of the orbital stabilization at the LC-wPBE level. The broadening of the HOMO–LUMO band gap for the  $T_1$  exciton compared to the charged ( $P^+$  and  $P^-$ ) states is associated with the inverted bond length alternation observed at this level. Neutral excitons have higher binding energies than polarons. However, the trends observed for solvation energies are completely reversed.

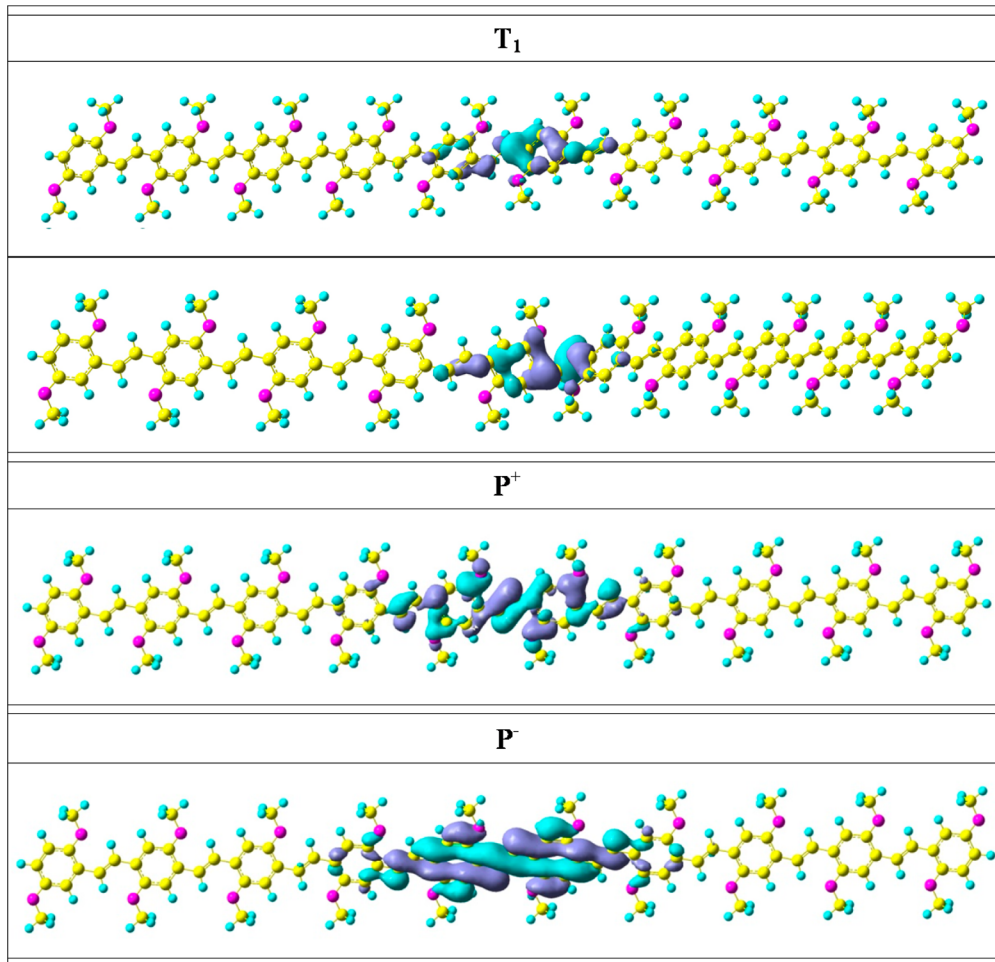


**Figure 7.** Characteristic natural orbitals (NOs) for the singly occupied electronic levels for the  $T_1$ ,  $P^+$ , and  $P^-$  excitations in their corresponding native geometries calculated at LC-wPBE/6-31G\* in the presence of solvent for the MEH-PPV oligomer composed of 10 repeat units. For  $T_1$ , only two orbitals shown have unit occupation. Whereas both  $P^+$  and  $P^-$  have only one NO each with a single occupation number.

LC-wPBE predicts the highest binding and solvation energies compared to other DFT levels used in this study. Thus, our investigation allows one to choose an appropriate electronic structure methodology and provides an analysis of the essential electronic excitations controlling energy-transfer and charge-transport processes in opto-electronic devices.

## ■ ASSOCIATED CONTENT

### S Supporting Information

Further details are given in Figures 1S–4S. This material is available free of charge via the Internet at <http://pubs.acs.org>.

## ■ AUTHOR INFORMATION

### Corresponding Author

\*E-mail: [serg@lanl.gov](mailto:serg@lanl.gov).

### Notes

The authors declare no competing financial interest.

## ■ ACKNOWLEDGMENTS

I.H.N., D.L.S., and R.L.M. acknowledge support of the DOE Office of Basic Energy Sciences (OBES) under Work Proposal Number 08SCPE973. S.T., A.S., and E.R.B. acknowledge support of the U.S. Department of Energy and Los Alamos National Laboratory (LANL) Directed Research and Development Funds. Los Alamos National Laboratory is operated by

Los Alamos National Security, LLC, for the National Nuclear Security Administration of the U.S. Department of Energy under contract DE-AC52-06NA25396.

## ■ REFERENCES

- (1) Wallukewitz, B. H.; Kabra, D.; Gelinas, S.; Friend, R. H. Triplet Dynamics in Fluorescent Polymer Light-Emitting Diodes. *Phys. Rev. B* **2012**, *85*, 045209.
- (2) AlSalhi, M. S.; Alam, J.; Dass, L. A.; Raja, M. Recent Advances in Conjugated Polymers for Light Emitting Devices. *Int. J. Mol. Sci.* **2011**, *12*, 2036–2054.
- (3) Chidichimo, G.; Filippelli, L. Organic Solar Cells: Problems and Perspectives. *Int. J. Photoenergy* **2010**, *123534*.
- (4) Hoppe, H.; Sariciftci, N. Organic solar cells: An overview. *J. Mater. Res.* **2004**, *19*, 1924–1945.
- (5) Peet, J.; Heeger, A. J.; Bazan, G. C. “Plastic” Solar Cells: Self-Assembly of Bulk Heterojunction Nanomaterials by Spontaneous Phase Separation. *Acc. Chem. Res.* **2009**, *42*, 1700–1708.
- (6) Ibnaouf, K. H. Laser from External Energy Transfer of MEH-PPV Conjugated Polymer. *Opt. Laser Technol.* **2012**, *44*, 710–713.
- (7) Samuel, I. D. W.; Turnbull, G. A. Organic Semiconductor Lasers. *Chem. Rev.* **2007**, *107*, 1272–1295.
- (8) Kergoat, L.; Piro, B.; Berggren, M.; Horowitz, G.; Pham, M.-C. Advances in Organic Transistor-Based Biosensors: From Organic Electrochemical Transistors to Electrolyte-Gated Organic Field-Effect Transistors. *Anal. Bioanal. Chem.* **2012**, *402*, 1813–1826.

- (9) Gemayel, M. E.; Treier, M.; Musumeci, C.; Li, C.; Mullen, K.; Samori, P. Tuning the Photoresponse in Organic Field-Effect Transistors. *J. Am. Chem. Soc.* **2012**, *134*, 2429–33.
- (10) Aryanpour, K.; Sheng, C. X.; Olejnik, E.; Pandit, B.; Psiachos, D.; Mazumdar, S.; Vardeny, Z. V. Evidence for Excimer Photoexcitations in an Ordered Pi-Conjugated Polymer Film. *Phys. Rev. B* **2011**, *83*, 155124.
- (11) Cabanillas-Gonzalez, J.; Grancini, G.; Lanzani, G. Pump-Probe Spectroscopy in Organic Semiconductors: Monitoring Fundamental Processes of Relevance in Optoelectronics. *Adv. Mater.* **2011**, *23*, S468–S485.
- (12) Dykstra, T. E.; Hennebicq, E.; Beljon, D.; Gierschner, J.; Claudio, G.; Bittner, E. R.; Knoester, J.; Scholes, G. D. Conformational Disorder and Ultrafast Exciton Relaxation in PPV-family Conjugated Polymers. *J. Phys. Chem. B* **2009**, *113*, 656–667.
- (13) Frolov, S. V.; Kloc, C.; Batlogg, B.; Wohlgemant, M.; Jiang, X.; Vardeny, Z. V. Excitation Dynamics in Single Molecular Crystals of Alpha-Hexathiophene from Femtoseconds to Milliseconds. *Phys. Rev. B* **2001**, *63*, 205203.
- (14) Clark, J.; Nelson, T.; Tretiak, S.; Cirmi, G.; Lanzani, G. Femtosecond torsional relaxation. *Nat. Phys.* **2012**, *8*, 225–31.
- (15) Thorsmølle, V. K.; Averitt, R. D.; Demsar, J.; Smith, D. L.; Tretiak, S.; Martin, R. L.; Chi, X.; Crone, B. K.; Ramirez, A. P.; Taylor, A. J. Morphology Effectively Controls Singlet-Triplet Exciton Relaxation and Charge Transport in Organic Semiconductors. *Phys. Rev. Lett.* **2009**, *102*, 017401.
- (16) Tretiak, S.; Chao, W.; Chernyak, V. Y. Excited States and Optical Response of a Donor-Acceptor Substituted Polyene: A TD-DFT Study. *Chem. Phys. Lett.* **2007**, *433*, 305–11.
- (17) Moses, D.; Dogariu, A.; Heeger, A. J. Ultrafast Detection of Charged Photocarriers in Conjugated Polymers. *Phys. Rev. B* **2000**, *61*, 9373–9379.
- (18) Etzold, F.; Howard, I. A.; Mauer, R.; Meister, M.; Kim, T. D.; Lee, K. S.; Baek, N. S.; Laquai, F. Ultrafast Exciton Dissociation Followed by Nongeminate Charge Recombination in PCDTBT:PCBM Photovoltaic Blends. *J. Am. Chem. Soc.* **2011**, *133*, 9469–9479.
- (19) Osterbacka, R.; Wohlgemant, M.; Shkunov, M.; Chinn, D.; Vardeny, Z. V. Excitons, Polarons, and Laser Action in Poly(p-Phenylene Vinylene) Films. *J. Chem. Phys.* **2003**, *118*, 8905–8916.
- (20) Kohler, A.; dos Santos, D. A.; Beljon, D.; Shuai, Z.; Bredas, J. L.; Holmes, A. B.; Kraus, A.; Mullen, K.; Friend, R. H. Charge Separation in Localized and Delocalized Electronic States in Polymeric Semiconductors. *Nature* **1998**, *392*, 903–906.
- (21) AlSalhi, M. S.; Ibnaouf, K. H.; Masilamani, V.; Yassin, O. A. Amplified Spontaneous Emission from Internal Energy Transfer Process in the Copolymer BEHP-co-MEH-PPV. *J. Lumin.* **2012**, *132*, 484–490.
- (22) McCamey, D. R.; van Schooten, K. J.; Baker, W. J.; Lee, S. Y.; Paik, S. Y.; Lupton, J. M.; Boehme, C. Hyperfine-Field-Mediated Spin Beating in Electrostatically Bound Charge Carrier Pairs. *Phys. Rev. Lett.* **2010**, *104*, 017601.
- (23) Frolov, S. V.; Bao, Z.; Wohlgemant, M.; Vardeny, Z. V. Multiple Pulse Transient Spectroscopy in Luminescent Pi-Conjugated Polymers. *Synth. Met.* **2001**, *116*, 5–7.
- (24) Meng, K.; Ding, Q.; Wang, S. F.; Gong, Q. H. Ultrafast Energy Transfer in Blended Polyphenothiazine/Polyphenylene Vinylene Film. *Chem. Phys. Lett.* **2011**, *515*, 155–158.
- (25) Traub, M. C.; Lakhwani, G.; Bolinger, J. C.; Vanden Bout, D.; Barbara, P. F. Electronic Energy Transfer in Highly Aligned MEH-PPV Single Chains. *J. Phys. Chem. B* **2011**, *115*, 9941–9947.
- (26) Becker, K.; Da Como, E.; Feldmann, J.; Scheliga, F.; Csanyi, E. T.; Tretiak, S.; Lupton, J. M. How Chromophore Shape Determines the Spectroscopy of Phenylene-Vinylenes: Origin of Spectral Broadening in the Absence of Aggregation. *J. Phys. Chem. B* **2008**, *112*, 4859–64.
- (27) Ghosh, H. Ground and Excited State Nonlinear Optical Properties of Poly(-Para Phenylene Vinylene). *Synth. Met.* **2008**, *158*, 320–329.
- (28) Kilina, S.; Batista, E. R.; Yang, P.; Tretiak, S.; Saxena, A.; Martin, R. L.; Smith, D. L. Electronic Structure of Self-Assembled Amorphous Polyfluorenes. *ACS Nano* **2008**, *2*, 1381–1388.
- (29) Sun, M. T.; Kjellberg, P.; Beenken, W. J. D.; Pullerits, T. Comparison of the Electronic Structure of PPV and its Derivative DIOXA-PPV. *Chem. Phys.* **2006**, *327*, 474–484.
- (30) Yang, P.; Batista, E. R.; Tretiak, S.; Saxena, A.; Martin, R. L.; Smith, D. L. Effect of Intramolecular Disorder and Intermolecular Electronic Interactions on the Electronic Structure of Poly-p-Phenylene Vinylene. *Phys. Rev. B* **2007**, *76*, 241201.
- (31) Tretiak, S.; Saxena, A.; Martin, R. L.; Bishop, A. R. Conformational Dynamics of Photoexcited Conjugated Molecules. *Phys. Rev. Lett.* **2002**, *89*, 09740.
- (32) Franco, I.; Tretiak, S. Electron-Vibrational Dynamics of Photoexcited Polyfluorenes. *J. Am. Chem. Soc.* **2004**, *126*, 12130–12140.
- (33) Karabunarliev, S.; Bittner, E. R. Polaron-Excitons and Electron-Vibrational Band Shapes in Conjugated Polymers. *J. Chem. Phys.* **2003**, *118*, 4291–4296.
- (34) Franco, I.; Tretiak, S. Electron-Vibrational Relaxation of Photoexcited Polyfluorenes in the Presence of Chemical Defects: A Theoretical Study. *Chem. Phys. Lett.* **2003**, *372*, 403–408.
- (35) Campbell, L. H.; Smith, D. L.; Tretiak, S.; Martin, R. L.; Neef, C. J.; Ferraris, J. R. Excitation Transfer Processes in a Phosphor-Doped Poly(p-Phenylene Vinylene) Light-Emitting Diode. *Phys. Rev. B* **2002**, *65*, 085210.
- (36) Igumenshchev, K. I.; Tretiak, S.; Chernyak, V. Y. Excitonic Effects in a Time-Dependent Density Functional Theory. *J. Chem. Phys.* **2007**, *127*, 114902.
- (37) Geskin, V. M.; Dkhissi, A.; Bredas, J. L. Oligothiophene Radical Cations: Polaron Structure in Hybrid DFT and MP2 Calculations. *Int. J. Quantum Chem.* **2003**, *91*, 350–354.
- (38) Tretiak, S.; Igumenshchev, K.; Chernyak, V. Exciton Sizes of Conducting Polymers Predicted by Time-Dependent Density Functional Theory. *Phys. Rev. B* **2005**, *71*, 033201.
- (39) Norton, J. E.; Bredas, J. L. Polarization Energies in Oligoacene Semiconductor Crystals. *J. Am. Chem. Soc.* **2008**, *130*, 12377–12384.
- (40) Nayyar, I. H.; Batista, E. R.; Tretiak, S.; Saxena, A.; Smith, D. L.; Martin, R. L. Localization of Electronic Excitations in Conjugated Polymers Studied by DFT. *J. Phys. Chem. Lett.* **2011**, *2*, 566–571.
- (41) Nguyen, T. D.; Hukic-Markosian, G.; Wang, F. J.; Wojcik, L.; Li, X. G.; Ehrenfreund, E.; Vardeny, Z. V. Isotope Effect in Spin Response of Pi-Conjugated Polymer Films and Devices. *Nat. Mater.* **2010**, *9*, 345–352.
- (42) Cornil, J.; Beljon, D.; Heller, C. M.; Campbell, I. H.; Laurich, B. K.; Smith, D. L.; Bradley, D. D. C.; Mullen, K.; Bredas, J. L. Photoluminescence Spectra of Oligo-Paraphenylenevinylenes: A Joint Theoretical and Experimental Characterization. *Chem. Phys. Lett.* **1997**, *278*, 139–145.
- (43) Kuroda, S. ESR and ENDOR studies of solitons and polarons in conjugated polymers. *Appl. Magn. Reson.* **2003**, *23*, 455–468.
- (44) Miranda, R. P.; Fisher, A. J.; Stella, L.; Horsfield, A. P.; Multiconfigurational Time-Dependent, A. Hartree-Fock Method for Excited Electronic States. II. Coulomb Interaction Effects in Single Conjugated Polymer Chains. *J. Chem. Phys.* **2011**, *134*, 244102.
- (45) Sai, N.; Barbara, P. F.; Leung, K. Hole Localization in Molecular Crystals from Hybrid Density Functional Theory. *Phys. Rev. Lett.* **2011**, *106* (22), 085210 (8).
- (46) Geskin, V. M.; Grozema, F. C.; Siebbeles, L. D. A.; Beljon, D.; Bredas, J. L.; Cornil, J. Impact of the Computational Method on the Geometric and Electronic Properties of Oligo(Phenylene Vinylene) Radical Cations. *J. Phys. Chem. B* **2005**, *109*, 20237–20243.
- (47) Zojer, E.; Buchacher, P.; Wudl, F.; Cornil, J.; Calbert, J. P.; Bredas, J. L.; Leising, G. Excited State Localization in Organic Molecules consisting of Conjugated and Nonconjugated Segments. *J. Chem. Phys.* **2000**, *113*, 10002–10012.
- (48) Bedard-Hearn, M. J.; Sterpone, F.; Rossky, P. J. Nonadiabatic Simulations of Exciton Dissociation in Poly-p-phenylenevinylene Oligomers. *J. Phys. Chem. A* **2010**, *114*, 7661–7670.

- (49) Frolov, S. V.; Bao, Z.; Wohlgemant, M.; Vardeny, Z. V. Ultrafast Spectroscopy of Even-Parity States in Pi-Conjugated Polymers. *Phys. Rev. Lett.* **2000**, *85*, 2196–2199.
- (50) Frisch, M. J.; Trucks, G. W.; Schlegel, H. B.; Scuseria, G. E.; Robb, M. A.; Cheeseman, J. R.; Scalmani, G.; Barone, V.; Mennucci, B.; Petersson, G. A.; Nakatsuji, H.; Caricato, M.; Li, X.; Hratchian, H. P.; Izmaylov, A. F.; Bloino, J.; Zheng, G.; Sonnenberg, J. L.; Hada, M.; Ehara, M.; Toyota, K.; Fukuda, R.; Hasegawa, J.; Ishida, M.; Nakajima, T.; Honda, Y.; Kitao, O.; Nakai, H.; Vreven, T.; Montgomery, Jr., J. A.; Peralta, J. E.; Ogliaro, F.; Bearpark, M.; Heyd, J. J.; Brothers, E.; Kudin, K. N.; Staroverov, V. N.; Kobayashi, R.; Normand, J.; Raghavachari, K.; Rendell, A.; Burant, J. C.; Iyengar, S. S.; Tomasi, J.; Cossi, M.; Rega, N.; Millam, N. J.; Klene, M.; Knox, J. E.; Cross, J. B.; Bakken, V.; Adamo, C.; Jaramillo, J.; Gomperts, R.; Stratmann, R. E.; Yazyev, O.; Austin, A. J.; Cammi, R.; Pomelli, C.; Ochterski, J. W.; Martin, R. L.; Morokuma, K.; Zakrzewski, V. G.; Voth, G. A.; Salvador, P.; Dannenberg, J. J.; Dapprich, S.; Daniels, A. D.; Farkas, Ö.; Foresman, J. B.; Ortiz, J. V.; Cioslowski, J.; Fox, D. J. *Gaussian-09*, Revision A.1; Gaussian Inc.: Wallingford, CT, 2009.
- (51) Tammer, M.; Monkman, A. P. Measurement of the Anisotropic Refractive Indices of Spin Cast Thin Poly(2-Methoxy-5-(2'-ethylhexyloxy)-p-Phenylenevinylene) (MEH-PPV) Films. *Adv. Mater.* **2002**, *14*, 210–212.
- (52) Perdew, J. P.; Burke, K.; Ernzerhof, M. Generalized Gradient Approximation Made Simple. *Phys. Rev. Lett.* **1997**, *78*, 1396–1396.
- (53) Becke, A. D. A New Mixing of Hartree-Fock and Local Density-Functional Theories. *J. Chem. Phys.* **1993**, *98*, 1372–1377.
- (54) Yanai, T.; Tew, D. P.; Handy, N. C. A New Hybrid Exchange-Correlation Functional using the Coulomb-Attenuating Method (CAM-B3LYP). *Chem. Phys. Lett.* **2004**, *393*, 51–57.
- (55) Vydrov, O. A.; Scuseria, G. E. Assessment of a Long-Range Corrected Hybrid Functional. *J. Chem. Phys.* **2006**, *125*, 074106.
- (56) Zheng, G.; Clark, S. J.; Brand, S.; Abram, R. A. First-Principles Studies of the Structural and Electronic Properties of Poly-Para-Phenylen Vinylene. *J. Phys.: Condens. Matter* **2004**, *16*, 8609–8620.
- (57) Moro, G.; Scalmani, G.; Cosentino, U.; Pitea, D. On the Structure of Polaronic Defects in Thiophene Oligomers: a Combined Hartree-Fock and Density Functional Theory Study. *Synth. Met.* **2000**, *108*, 165–172.
- (58) Sears, J. S.; Koerzdoerfer, T.; Zhang, C.-R.; Bredas, J.-L. Communication: Orbital Instabilities and Triplet States from Time-Dependent Density Functional Theory and Long-Range Corrected Functionals. *J. Chem. Phys.* **2011**, *135*, 151103.
- (59) Magyar, R. J.; Tretiak, S. Dependence of Spurious Charge-Transfer Excited States on Orbital Exchange in TDDFT: Large Molecules and Clusters. *J. Chem. Theory Comput.* **2007**, *3*, 976–987.
- (60) Martin, R. L. Natural Transition Orbitals. *J. Chem. Phys.* **2003**, *118*, 4775–4777.
- (61) Wu, C.; Malinin, S.; Tretiak, S.; Chernyak, V. Exciton Scattering and Localization in Branched Dendrimeric Structures. *Nat. Phys.* **2006**, *2*, 631–635.
- (62) Suponitsky, K. Y.; Masunov, A. E.; Antipin, M. Y. Computational Search for Nonlinear Optical Materials: Are Polarization Functions Important in the Hyperpolarizability Predictions of Molecules and Aggregates? *Mendeleev Commun.* **2009**, *19*, 311–313.
- (63) Masunov, A.; Tretiak, S.; Hong, J. W.; Liu, B.; Bazan, G. C. Theoretical Study of the Effects of Solvent Environment on Photophysical Properties and Electronic Structure of Paracyclophane Chromophores. *J. Chem. Phys.* **2005**, *122*, 224505.
- (64) Brendel, P.; Grupp, A.; Mehring, M.; Schenck, R.; Mullen, K.; Huber, W. Chain Length-Dependent Polaron ( $P^-$ ) Width in Phenylene Oligomers - A Solid-State ENDOR Investigation. *Synth. Met.* **1991**, *45*, 49–57.
- (65) Bredas, J. L.; Themans, B.; Fripiat, J. G.; Andre, J. M.; Chance, R. R. Highly Conducting Polyparaphenylene, Polypyrrole, and Polythiophene Chains - An Ab initio Study of the Geometry and Electronic-Structure Modifications upon Doping. *Phys. Rev. B* **1984**, *29*, 6761–6773.
- (66) Brocks, G. Polarons and Bipolarons in Oligothiophenes: A First Principles Study. *Synth. Met.* **1999**, *102*, 914–915.
- (67) Geskin, V. M.; Cormil, J.; Bredas, J. L. Comment on “Polaron formation and Symmetry Breaking” by L Zuppiroli et al. *Chem. Phys. Lett.* **2005**, *403*, 228–231.
- (68) Zuppiroli, L.; Bieber, A.; Michoud, D.; Galli, G.; Gygi, F.; Bussac, M. N.; Andre, J. J. Polaron Formation and Symmetry Breaking. *Chem. Phys. Lett.* **2003**, *374*, 7–12.
- (69) Jianmin, T.; Tretiak, S.; Jian-Xin, Z. Performance of a Nonempirical Meta-Generalized Gradient Approximation Density Functional for Excitation Energies. *J. Chem. Phys.* **2008**, *128*, 084110.